Conception and Design of a Dual-Property Haptic Stimuli Database Integrating Stochastic Roughness and Elasticity

Karina Kirk Driller[1,2(✉)], Camille Fradet[2], Vincent Hayward[1], and Jess Hartcher-O'Brien[3]

[1] Sorbonne University, 75005 Paris, France
karina.driller@sorbonne-universite.fr
[2] Delft University of Technology, 2628 CE Delft, The Netherlands
[3] Reality Labs Research, Meta, Redmond, WA 98052, USA

Abstract. Understanding the interplay between surface roughness and material elasticity in haptic texture perception is important. In the real world, these characteristics do not occur isolated from one another, yet, the haptic perceptions of surface features and material properties are often investigated individually. This highlights the need for suitable stimulus material for haptic perceptual experiments. The present research details the manufacturing and validation of a database of stochastically-rough, elastic stimuli tailored for haptic perceptual experiments. The stimulus set comprises 49 3D-printed samples, offering a systematic variation in stochastic microscale roughness and material elasticity, replicating natural surface features without compromising experimental control. The surfaces were generated using an algorithm that produces randomly rough surfaces with well-defined spectral distributions, demonstrating fractal properties over a large range of length scales. Controlled variations in elasticity were implemented via variations of the printing material composition. Finally, we present preliminary perceptual data from two observers, illustrating the discriminability of the stimulus space for roughness and softness discrimination. This database aims to facilitate haptic research on material and texture perception, offering a controlled yet naturalistic set of stimuli to explore the intricate interplay between surface roughness and material elasticity in shaping haptic texture perception.

Keywords: Haptic texture database · Cue combination · Surface roughness · Material elasticity

1 Introduction

Most natural and engineered surfaces that we encounter during our everyday life, are self-affine surfaces, exhibiting fractal properties over a range of length scales

K. K. Driller and C. Fradet—These authors contributed equally to this research.

H. Kajimoto et al. (Eds.): EuroHaptics 2024, LNCS 14769, pp. 223–237, 2025.
https://doi.org/10.1007/978-3-031-70061-3_19

[1]. However, research on the perception of surface roughness has typically used simpler stimulus material (such as sandpapers or sinusoidal gratings) that can be varied easily in a controlled fashion (e.g., [2–5]). Furthermore, surface roughness tends to occur alongside other texture or material dimensions, such as material elasticity [6–8]. While the haptic perception of surface roughness and material elasticity (softness/hardness) have each been investigated extensively, the need for investigating the combined effects of different cues on perceptual outcomes is often stressed (e.g., [9]). More specifically, there is recent evidence suggesting that material elasticity and surface structure are sometimes not perceived independently [10]. While insightful, this research has employed relatively simple stimulus material, not reflecting the often complex nature of both engineered and natural surfaces. Conversely, when using databases of naturally occurring textures and materials (e.g., [6]) research faces a multitude of physical cues difficult to control in an experimental setting. This stresses the need for behaviourally-relevant yet well-controlled stimulus material for haptic research on texture and material perception. Here we therefore present a database of 3D-printed stimuli varying systematically in their microscale roughness and material elasticity, intended for haptic perceptual experiments. The presented stimuli resemble natural textures in their surface statistics by exhibiting self-affine fractal properties over a range of length scales relevant to touch, while not compromising on the experimental control needed due to thorough characterization. The database consists of seven different surfaces varying in their scale-dependent roughness (Hurst exponent) on a 0.03–5 mm scale, each available in seven different elasticities - together resulting in a final database of 49 3D-printed samples.

The surfaces in this database were generated using an algorithm that produces randomly-rough surfaces with well-defined spectral distributions [11,12], exhibiting fractal properties as described by Persson [1]. These surfaces are produced by a superposition of waves, where the amplitudes are derived from a height-spectrum which is composed of a plateau for large wavelengths of equal amplitude (defining the macroscopic topography) while amplitudes of smaller wavelengths (defining the microscale topography) decay according to a power-law. A smaller Hurst exponent, H, leads to a slower decay towards small length scales and thus results in a higher microscale roughness. This hyperbolic decay in topography wavelengths is expected to impose a similar pattern in the temporal spectral content of the friction-elicited vibrations during an interaction. Indeed, it has been observed that some spatial spectral properties of textures, like the hyperbolic wavelengths decay, are transmitted to the spectral content of the vibrotactile signal [13,14]. Randomness is implemented in the phase shift between the superposed waves which is controlled by a random number sequence. The final topographies are obtained by combining the parametrised spectrum and the random phase shift into a spatial frequency representation and applying an inverse Fourier transform. For the present sample set, the macroscale topography remained the same for all samples, as recent research has demonstrated such larger-scale topographic differences or “higher order statistics” to be of little relevance for tactile texture perception [15–17]. The Hurst exponent, H, on

the other hand, has been shown to be a perceptually-relevant parameter for the discrimination of roughness using the same surface algorithm, albeit on much larger length scales [17].

2 Methods

2.1 Generation of Surfaces

For the stimuli of the database presented here, the slope of the function for shorter wavelengths was varied in seven steps, spanning an H from 0.3 to 0.9 m while the random sequence remained the same. This resulted in seven surfaces with the same 'macroscale' topography but varying in their 'microscale' roughness or self-affinity. The longest wavelength was set to the longest side of the final stimuli (50 mm) while the shortest possible wavelength was set to 0.03 mm. This value was chosen because the Polyjet 735 used for 3D printing of the stimuli has the resolution of 0.0135 mm. Following the Nyquist-Shannon sampling theorem, it was therefore expected that it could present details down to approximately 0.027 mm. To create comparatively smooth (not rugged) stimuli, with little variation in the large wavelengths, the roll-off wavelength was set to a value of 5 mm, approximately corresponding to half of an average fingertip width. This value defined the cut-off between the plateau and the interval of wavelengths that the fractal dimension was applied to. The surfaces generated were 50×50 mm (note that one of the sides was later cropped to 31 mm for the final 3D-printed samples). Figure 1 displays the model used from Müser et al. [12] to design the height spectrum of the generated surfaces and the steps taken to generate the surface topographies.

The global scale of the wavelength amplitude C_0 (Fig. 1A) was set to 1 for all seven topographies generated. The spectra (Fig. 1B) were then used to create a 2D spectral content of 3704×3704 samples. An inverse Fourier transform was applied using an inverse fast Fourier transform algorithm and the result was then multiplied by $\frac{N^2}{2\pi}$, with N being the number of samples per dimension (3704). We then scaled the obtained topographies by 0.01, to generate topographic details of relevant size. This scaling factor was selected based on 3D-visualizations as well as pilot discrimination studies of test stimuli, as we wished to produce stimuli with an approximate step size in change of a JND (just-noticeable difference) in perceived roughness. Contrary to Sahli et al. [17], we multiplied all topographies by the same factor. This resulted in the seven topographies having the same amplitude for the wavelengths larger than the roll-off value, but a root mean square of heights decreasing with an increasing H value. This decision was based on perceptual pilot studies not reported here. The height matrices obtained were 50×50 mm, both dimensions with a sampling rate of 74.08 samples per millimetre (3704 samples for 50 mm). They were then cropped along one dimension to obtain 50×31 mm (3704×2296 samples). The spatial definition was set very high to match the theoretical minimum droplet size of the 3D printer, enabling the capture of microscale details at the closest possible approximation to their limits. The height matrices were then transformed to STL files

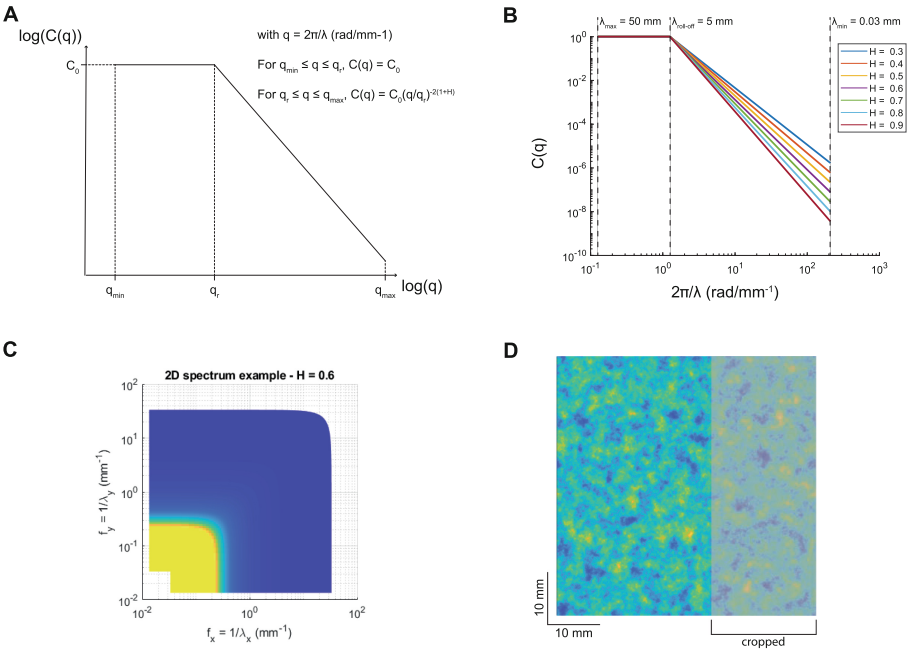

Fig. 1. Topography generation. (A) The spatial spectrum model from Müser et al. [12]. (B) Parametrisation of the spatial spectrum for the 7 surfaces of the present set. (C) An example of the resulting 2D-spectrum (here showing only the strictly positive frequencies quarter, in log space which distorts the expected shape of the spectrum) obtained from $H = 0.6$. (D) The resulting topography obtained by applying an inverse Fourier transform to the example spectrum shown in graph C.

in python by loading the height matrices from a configuration file, converting them into 3D surfaces represented by vertices and then generating triangles by dividing each rectangular area between adjacent vertices into two triangles. The resulting mesh was then saved to an STL file. Since this produced file sizes larger than needed, we used the "Quadric Edge Collapse Decimation" simplification function of MeshLab to decimate each sample with a decimation ratio of 6% (quality threshold 0.6; options "Preserve Boundary of the mesh", "Preserve Normal", "Preserve Topology" applied). The quality threshold was set to 0.6 and the following settings were applied: "Preserve Boundary of the mesh", Preserve Normal", and "Preserve Topology". These parameters were chosen with respect to a minimal deviation between the initial and decimated STL files, as estimated using the Hausdorff Distance sampling method (deviation in % of diagonal of 3D object: max 0.025946, mean 0.00336, rms 0.004386). Although minimal, this decimation may have resulted in a slight smoothing effect on the STL files compared to the original height matrices.

2.2 3D Printing

Each of these seven surfaces were then 3D printed in seven different elasticities using a Connex Stratasys Polyjet J735 with the printer software (GrabCAD Print 1.60.9.13125). Different elasticities were achieved by combining the rigid *VeroYellow*^{TM} and the flexible *Agilus30*^{TM} in the proportions predefined by the printer software for Shore-A values 30, 35, 40, 50, 60, 70, and 85 (but see Table 1 for achieved shore-A values). All stimuli were sized $50 \times 31 \times 13$ mm including a rigid platform of 3 mm which was CAD-modelled underneath each stimulus in *VeroMagenta*^{TM} to provide a stable base for the samples and for engraved text for identification of the stimuli. The stimuli were printed in glossy finish. However, to avoid head-bumper impacts during the printing process, as well as to achieve more flexible (i.e., more elastic) stimuli than standard settings allow, the 3D prints were printed with only half of the amount of UV-curing normally used (by enabling only one of the two UV lamps of the printer) and post-cured in a curing device (Formlabs Form Cure) for 30 s at an LED Radiant wattage of 9.1 W and an LED Wavelength 405 nm[1]. This resulted in a final database of 49 samples (see Fig. 2).

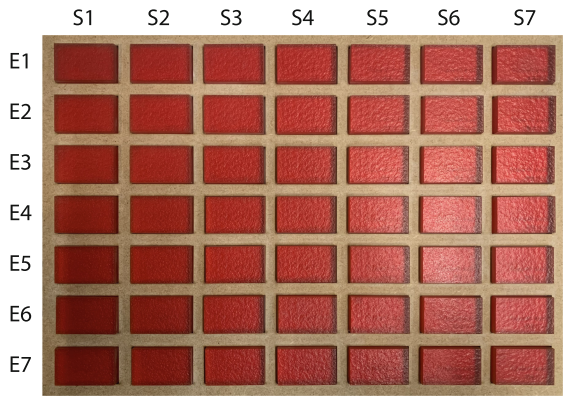

Fig. 2. Image of the final database of 49 samples. Columns (S1-7) indicate changes in the surface statistics, corresponding to an H between 0.3 and 0.9. Rows (E1-7) indicate changes in the elasticity, (cf. Table 1). All samples measure $50 \times 31 \times 13$ mm (including the rigid platform below the flexible prints).

[1] The thickness of the stimuli and their comparatively flat surface leads to a large contact area with the roller of the printer, which increases the risk of head-bumper impacts, especially for the more flexible prints, where the roller cannot scrape away enough material and unwanted material gets stuck. Less curing results in the surface becoming less sticky during the printing process.

2.3 Verification Procedure of the 3D-Printed Samples

After fabrication, the samples were measured with a shore-A durometer (Teclock GS-709N) on their long axis for 20 s at a temperature of approximately 20°C. The Young's modulus was thereafter calculated using Gent's conversion equation [18]. Table 1 summarizes the defined and achieved elasticity parameters of the database.

Table 1. Elasticity parameters of the database. The shore-A values were measured with a shore-A durometer on the centre of their long axis for 20 s. The values are the mean across all 7 surfaces, standard deviation in parenthesis. Young's moduli were calculated using Gent's conversion equation [18].

Elast. Nr.	E1	E2	E3	E4	E5	E6	E7
Shore A Target	30	35	40	50	60	70	85
Shore A Achieved	23.6 (0.55)	24.83 (0.41)	25.83 (0.41)	28.67 (0.52)	34 (0.71)	44.2 (1.48)	65.8 (1.1)
Y. Modulus (MPa)	0.121	0.122	0.128	0.144	0.179	0.264	0.611

To verify the surface statistics of the final 3D-printed stimuli, profilometry measurements were carried out on a subset of the samples. A key aim of this was to ensure that changes in the elasticity of the samples did not result in significant changes of the surface features. Due to the respective advantages and disadvantages of contact and optical profilometry, different subsets of the database were subjected to each of these methods. A smaller subset of five samples underwent contact profilometry. This method provided accurate topographical data of the same central location of different samples, allowing us to compare these directly. With this method we could furthermore be sure that differences in translucency of the samples (resulting from the different mixing ratios of the two different printing materials) would not affect the measurements. Optical profilometry measurements were carried out on a larger subset of nine samples, with three repeated measurements of each sample at random locations, allowing for overall conclusions about surface statistics and roughness parameters.

Contact profilometry measurements were carried out for surfaces S1 (H = 0.3), S4 (H = 0.6), and S7 (H = 0.9) at the medium elasticity of the parameter space (E4). To investigate the consistency of the topography over different elasticities, further measurements were taken on elasticities E1 and E7 of surface S4 (cf. Fig 2). Two of the surfaces (S4E4 and S4E7) were measured twice to estimate the test-retest reliability. The measurements were made using a Dektak 150 Surface Profiler. All measurements were taken in the centre 5×5 mm of the surfaces, by taking the line crossing of diagonals drawn from the corners. The distance between each line of measurements was 30µm while the distance between each measurement point was 4 µm. Plots of the measured as compared to theoretical (before decimation and 3D printing) height data can be seen in Fig. 3.

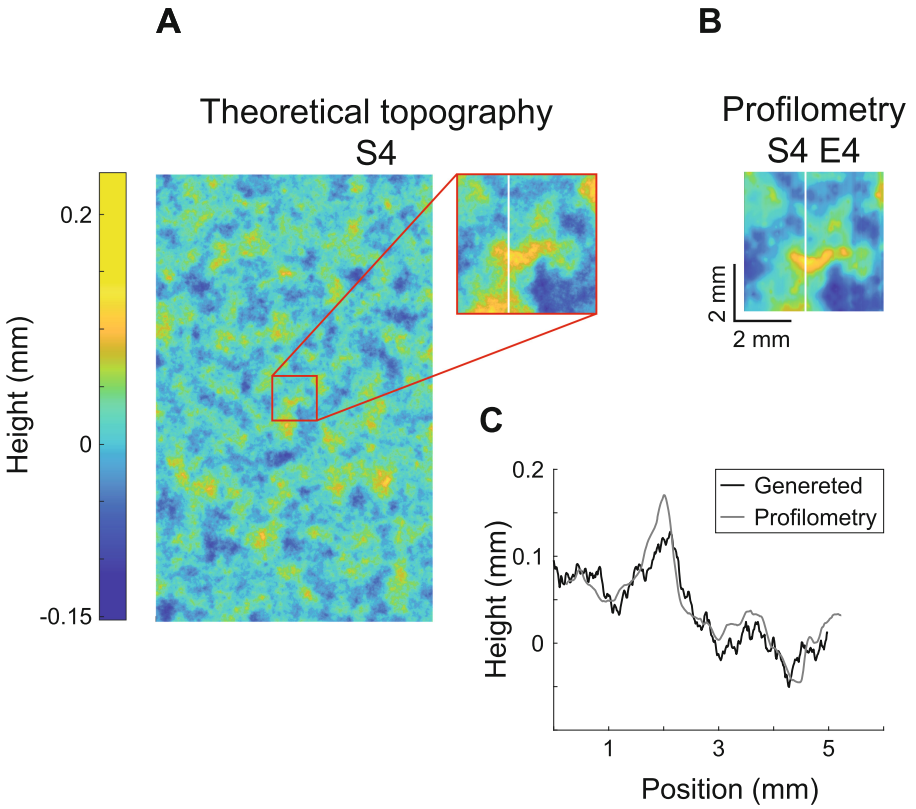

Fig. 3. (A) Top view of example theoretical topography S4 (H = 0.6) (height spectrum generated before decimation 3D and 3D printing). The red square indicates the corresponding 5×5 mm window in which contact profilometry measurements were carried out on the 3D-printed stimuli. (B) Plots of the height data achieved from the contact profilometry of the corresponding location on the same surface 3D printed at medium elasticity. (C) Profile view comparison between the theoretical and measured height data at matched coordinates. The position of the profile cut is indicated by a white line om graphs A and B. (Color figure online)

Figure 3 demonstrates the great resemblance between theoretical and measured height data. On Fig. 3C a certain amount of "smoothing out" of the finest details in the profile of the final 3D print is visible. While the height profiles follow the target topography closely, detail and prominence of the asperities is lost for the very smallest variations. This smoothing effect mainly concerns details within the micrometer range, however, and is to be expected due to the (A) the decimation of the STL files and more importantly (B) the limited resolution of the 3D printer.

Optical profilometry was carried out on samples S1 (H = 0.3), S4 (H = 0.6), and S7 (H = 0.9) at elasticities E1, E4 and E7 (cf. Fig. 2). On each of

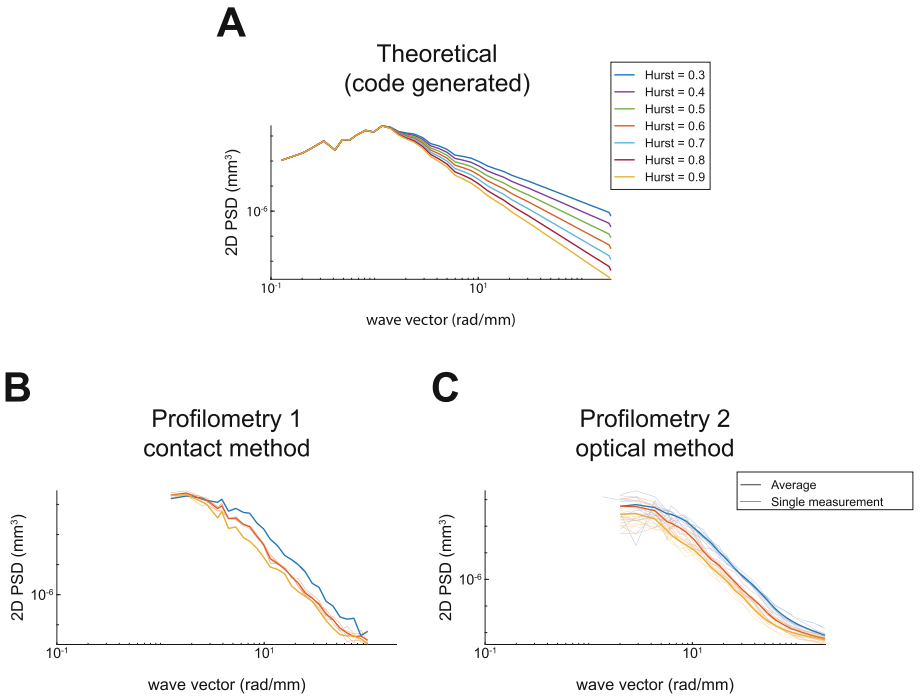

Fig. 4. Height power-spectral density of (A) the 7 theoretical surfaces (before triangulation, decimation, and 3D printing), (B) contact-profilometry measurements of the 5×5 mm window of 5 chosen final samples and (C) optical profilometry measurements. The radial direction is used for all plots.

these samples, 3 different measurements were taken at 3 random locations. The measurements were made using a MarSurf CM Explorer. Each measurement comprised a 3.1×3.1 mm window. The lateral resolution was 1.33 µm at 10X with the pixel arrangement being 1200×1200 for a single scan. The measuring-vertical range with the fine motor was 0.35 mm.

We used an online tool [19] to analyse all profilometry measurements (contact and optical) and the theoretical topographies. Figure 4 shows the height power-spectral density of the theoretical topographies and measurements of the final surfaces respectively. As anticipated, a clear downward slope in frequency can be observed, changing with H. There is a clear difference in the power spectral density (PSD) from one H to another.

We then calculated the 2D RMS heights (known as Rq or Sq for the roughness of a surface), the RMS slope (gradient, RΔq), and the RMS curvature for all measurements. The values from the profilometry measurements were then compared to the values of all original theoretical surface files. Figure 5 and Table 2 summarize these data.

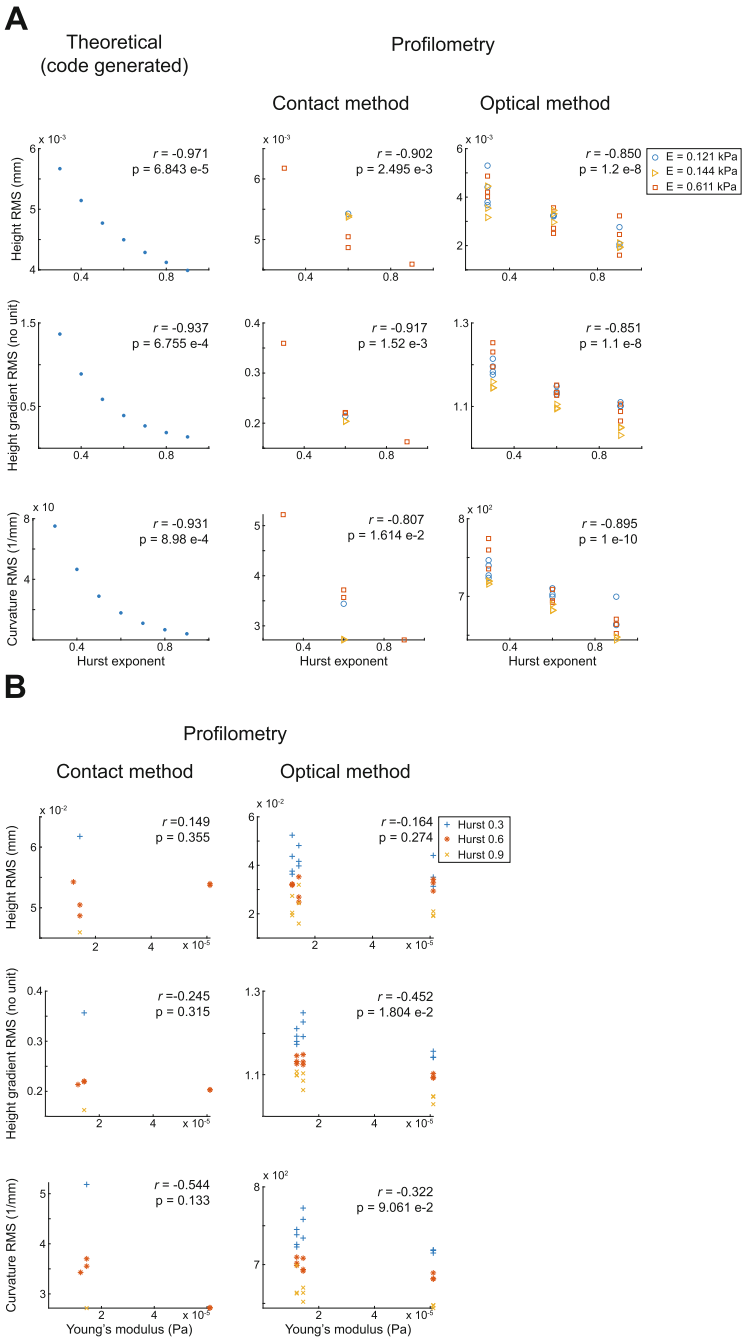

Fig. 5. (A) The root mean square of heights (Rq), the root mean square of slope (gradient, RΔq), and the root mean square of the curvature, for contact profilometry, optical profilometry and the theoretical topographies as a function of H. r = Pearson's correlation coefficient for the relationship between H and the respective roughness statistic. (B) The same statistics as a function of the sample elasticity.

Table 2. Roughness parameters of theoretical topographies and profilometry measurements of 3D-printed stimuli. Rq = RMS height, RΔq = RMS slope. Measurements from contact profilometry are displayed in bold.

Surface nr. (H)		S1 (H 0.3)	S2 (H 0.4)	S3 (H 0.5)	S4 (H 0.6)	S5 (H 0.7)	S6 (H 0.8)	S7 (H 0.9)
Theoretical Rq $\left[\times 10^{-2}\, mm\right]$		5.68	5.16	4.79	4.51	4.3	4.14	4.01
Profilometry 1 R_q $\left[\times 10^{-2}\, mm\right]$ Profilometry 2 Rq $\left[\times 10^{-2}\, mm\right]$	E1	3.8 3.67 5.3 4.41	N/A	N/A	**5.43** 3.21 3.24 3.26	N/A	N/A	2.06 1.95 2.76
	E4	**6.18** 4.02 4.21 4.87	N/A	N/A	**4.87** **5.05** 2.5 3.56 2.71	N/A	N/A	**4.59** 1.61 2.56 3.23
	E7	3.54 3.16 4.45	N/A	N/A	**5.37** **5.39** 3.45 2.96 3.31	N/A	N/A	2.11 1.92 1.94
Theoretical RΔq (gradient)		1.38	0.9	0.6	0.4	0.28	0.2	0.15
Profilometry 1 RΔq (gradient) profilometry 2 RΔq (gradient)	E1	1.18 1.18 1.21 1.20	N/A	N/A	**0.21** 1.13 1.13 1.15	N/A	N/A	1.10 1.11 1.10
	E4	**0.36** 1.25 1.23 1.19	N/A	N/A	**0.22** **0.22** 1.15 1.13 1.13	N/A	N/A	**0.16** 1.09 1.07 1.11
	E7	1.14 1.14 1.16	N/A	N/A	**0.2** **0.2** 1.10 1.11 1.09	N/A	N/A	1.03 1.05 1.05
Theoretical rms curvature [mm-1]		75.72	47.16	29.45	18.44	11.59	7.31	4.63
Profilometry 1 rms curvature [mm-1] Profilometry 2 rms curvature [mm-1]	E1	723.76 727.06 746.54 739.71	N/A	N/A	**3.44** 702.56 699.72 710.40	N/A	N/A	664.14 699.60 663.07
	E4	**5.22** 774.49 759.73 735.37	N/A	N/A	**3.57** **3.72** 709.06 694.34 692.33	N/A	N/A	**2.72** 663.98 652.23 670.65
	E7	719.12 715.84 719.96	N/A	N/A	**2.73** **2.72** 682.33 689.89 681.91	N/A	N/A	643.98 647.36 647.86

As can be seen in Fig. 5A, the Rq values of profilometry measurements follow the predicted pattern, where a lower H leads to a higher Rq. The Pearson correlation coefficient is significant and indicates a strong relationship for both profilometry measurements (contact and optical). The same holds true for the root mean square of slope and curvature, although some grouping of the samples with different elasticities can be observed. This variance between samples of different elasticities is not larger than the variance observed for repeated

measurements of the same sample, however, but is within the general level of measurement noise, which expectedly increases as derivatives are applied. Such a degree of variance is expected, not the least due to the changes in measurement location during the optical profilometry. It must furthermore be noted for the contact profilometry data, that, although the centre of the surface was targeted for each measurement, slight offsets will likely be present as the samples were marked and placed by hand (cf. Fig. 3). This is a likely source of noise, especially on the RMS of heights which, at this scale, will be highly sensitive to the exact position of measurement. Figure 5B demonstrates how changes in the elasticity of the samples do not result in a corresponding change in any of the roughness statistics. All Pearson correlation coefficients are below significance level.

It must be noted, that although these measurements testify to a significant relationship between the H and the measured roughness statistics (i.e., rms height, gradient and curvature) for both profilometry measurements, a considerable difference in absolute roughness values between the theoretical topographies and the measurements of the 3D-printed samples is present, which increases as the degree of derivation increases. A similar difference can be observed between the contact and optical profilometry measurements, where the difference between the two methods is very small for the RMS of heights but increases strongly with successive derivation. This discrepancy might very well be due to the broader bandwidth in the optical method, capturing more noise and the physical limitations of the contact method's stylus missing fine details. As a general matter, the difficulty to capture the topographies of the samples presented here lies in their very nature. They are defined on a large wavelength interval and display a relatively large range of asperity sizes. Each measurement method will introduce errors of different nature affecting the spectrum differently and the derivatives will increase these relative errors. This is expected to have led to a deprecation of the small wavelengths representations and to have affected the statistics of the surface as we applied derivatives. Importantly however, the profilometry enabled us to verify the relative differences between the different surfaces, quantifying the preservation of the significant correlation between variations in H and the resulting roughness statistics.

3 Perceptual Validation

We conducted a pilot study involving two observers to evaluate the utility of the database and to demonstrate the perceptual relevance of the stimuli. To gain comprehensive insights into the entire stimulus space, we employed an active learning paradigm called AEPsych [20]. This approach uses non-parametric Gaussian Process models to efficiently estimate psychometric fields by dynamically adjusting experimental conditions based on the responses from previous trials. It thereby optimizes the information gained per trial and increases threshold estimation efficiency across two or more stimulus dimensions (e.g., the Hurst exponent and elasticity).

The data presented are solely intended to illustrate the general discriminability of the stimulus space. Specifics of the procedure and the model's configuration are not detailed here.

In brief, data collection involved a two-alternative forced choice (2AFC) task for our 2D stimulus space, once for softness discrimination, using pressing with the index finger, and once for roughness discrimination, using lateral stroking. Each observer completed 50 trials for each task, during which they determined which one of two stimuli (as selected by the algorithm) felt rougher or softer respectively. Visual and auditory cues were removed for each observer. Observers provided written informed consent prior to participation, and the study adhered to the ethical guidelines of the Sorbonne University and the Helsinki Declaration.

Estimated psychometric fields are displayed in Fig. 6 for each observer and task.

As can be seen in Fig. 6, roughness and softness of the stimuli are distinctly discriminable within the stimulus space, where changes in the surface features coincide with changes in the perceived roughness of the surface while changes the elasticity coincide with changes in the perceived softness of the stimuli. The perceptual space of both observers is highly similar. In addition, there are regions

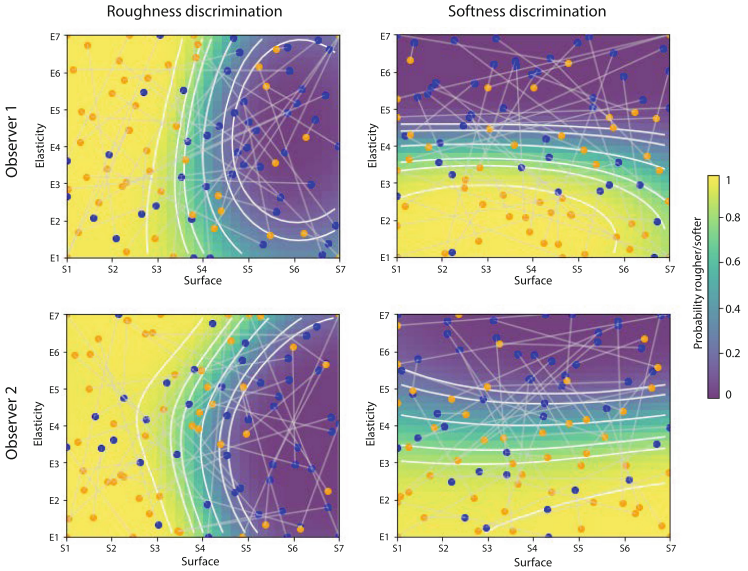

Fig. 6. Estimated psychometric fields for two participants for roughness discrimination (left) and softness discrimination (right). These plots show the probability of any stimulus within the 2D stimulus space being perceived as rougher or softer as compared to the midpoint of the stimulus space (S4, E4). Isocontours represent probability lines at 0.16, 0.25, 0.5, 0.75, 0.84, and 0.96 and can be interpreted in a similar manner as just-noticeable difference (JNDs). Each point-pair linked by a gray line represent the actual stimulus pairs chosen by the algorithm, where the orange point corresponds to the stimulus chosen as rougher/softer by the observer. (Color figure online)

in the space, unique to each observer where perceived roughness is influenced by both surface cues and material elasticity. These confounded cue regions are indicated by the isocontours in Fig. 6, left panel.

4 Availability of the Stimuli Database

The STL files for the stimuli described in this document are accessible on Dryad [DOI: 10.5061/dryad.j0zpc86nv]. To replicate the dual-property stimuli database as detailed here, it is necessary to 3D print all seven files in seven different material compositions as specified in Sect. 2.2. We caution researchers that achieving highly precise microscale features with variable elasticities must not be taken for granted. Deviations from the described printing procedures may lead to different outcomes.

5 Conclusion

In conclusion, the 3D-printed stimuli of our database represent a naturalistic and behaviourally-relevant, yet controlled set of samples for haptic texture perception research. The stimuli exhibit systematic variations in both surface roughness (as defined by the Hurst exponent H) and material elasticity. The profilometry measurements demonstrate a strong correlation between H and the measured roughness parameters for both contact and optical profilometry. Pilot perceptual data confirm the perceptual relevance of the stimuli database, suggesting that our database can provide a useful tool for investigating the interplay between surface roughness, material elasticity, and haptic texture perception.

Acknowledgments. We thank Roland Bennewitz and his team for providing the surface generation algorithm and for the optical profilometry measurements. We thank Joris van Dam for his assistance on the 3D-printing process as well as Nazih Mechbal and Cyril Gorny (Laboratoire PIMM) for their assistance on the contact profilometry. We acknowledge the funding from the European Union's Horizon 2020 research and innovation programme under the Marie Skłodowska-Curie Actions - Innovative Training Networks grant agreement H-Reality No 801413.

Disclosure of Interests. The authors have no competing interests to declare that are relevant to the content of this article.

References

1. Persson, B.N.J.: On the fractal dimension of rough surfaces. Tribol. Lett. **54**(1), 99–106 (2014). https://doi.org/10.1007/s11249-014-0313-4
2. Verrillo, R.T., Bolanowski, S.J., McGlone, F.P.: Subjective magnitude of tactile roughness. Somatosens. Motor Res. **16**(4), 352–360 (1999). https://doi.org/10.1080/08990229970401
3. Hollins, M., Risner, S.R.: Evidence for the duplex theory of tactile texture perception. Percept. Psychophys. **62**(4), 695–705 (2000). https://doi.org/10.3758/bf03206916
4. Libouton, X., Barbier, O., Plaghki, L., Thonnard, J.-L.: Tactile roughness discrimination threshold is unrelated to tactile spatial acuity. Behav. Brain Res. **208**(2), 473–478 (2010). https://doi.org/10.1016/j.bbr.2009.12.017
5. Yoshioka, T., Gibb, B., Dorsch, A.K., Hsiao, S.S., Johnson, K.O.: Neural coding mechanisms underlying perceived roughness of finely textured surfaces. J. Neurosci.: Off. J. Soc. Neurosci. **21**(17), 6905–6916 (2001). https://doi.org/10.1523/JNEUROSCI.21-17-06905.2001
6. Bergmann Tiest, W.M., Kappers, A.M.L.: Analysis of haptic perception of materials by multidimensional scaling and physical measurements of roughness and compressibility. Acta Physiol. (Oxf.) **121**(1), 1–20 (2006). https://doi.org/10.1016/j.actpsy.2005.04.005
7. Hollins, M., Bensmaïa, S., Karlof, K., Young, F.: Individual differences in perceptual space for tactile textures: evidence from multidimensional scaling. Percept. Psychophys. **62**(8), 1534–1544 (2000). https://doi.org/10.3758/BF03212154
8. Okamoto, S., Nagano, H., Yamada, Y.: Psychophysical Dimensions of Tactile Perception of Textures. IEEE Trans. Haptics **6**(1), 81–93 (2013). https://doi.org/10.1109/TOH.2012.32
9. Ernst, M.O., Bülthoff, H.H.: Merging the senses into a robust percept. Trends Cogn. Sci. **8**(4), 162–169 (2004). https://doi.org/10.1016/j.tics.2004.02.002
10. Gedsun, A., Sahli, R., Meng, X., Hensel, R., Bennewitz, R.: Bending as key mechanism in the tactile perception of fibrillar surfaces. Adv. Mater. Interfaces **9**(4), 2101380 (2022). https://doi.org/10.1002/admi.202101380
11. Müser, M., Dapp, W.B.: The contact mechanics challenge: problem definition. arXiv Soft Condensed Matter (2015). https://www.semanticscholar.org
12. Müser, M.H., et al.: Meeting the contact-mechanics challenge. Tribol. Lett. **65**(4), 118 (2017). https://doi.org/10.1007/s11249-017-0900-2
13. Bensmaia, S., Hollins, M.: The vibrations of texture. Somatosens. Mot. Res. (2003). https://doi.org/10.1080/0899022031000083825
14. Wiertlewski, M., Hudin, C., Hayward, V.: On the 1/f noise and non-integer harmonic decay of the interaction of a finger sliding on flat and sinusoidal surfaces. In: Proceedings of the 2011 World Haptics Conference (2011). https://doi.org/10.1109/WHC.2011.5945456
15. Kuroki, S., Sawayama, M., Nishida, S.: Haptic metameric textures. bioRxiv 653550 (2019). https://doi.org/10.1101/653550
16. Kuroki, S., Sawayama, M., Nishida, S.: The roles of lower- and higher-order surface statistics in tactile texture perception. J. Neurophysiol. **126**(1), 95–111 (2021). https://doi.org/10.1152/jn.00577.2020
17. Sahli, R., et al.: Tactile perception of randomly rough surfaces. Sci. Rep. **10**(1), 15800 (2020). https://doi.org/10.1038/s41598-020-72890-y

18. Gent, A.N.: On the relation between indentation hardness and young's modulus. Rubber Chem. Technol. **31**(4), 896–906 (1958). https://doi.org/10.5254/1.3542351
19. Röttger, M.C., et al.: Contact.engineering-create, analyze and publish digital surface twins from topography measurements across many scales. Surf. Topogr.: Metrol. Properties **10**(3), 035032 (2022). https://doi.org/10.1088/2051-672X/ac860a
20. Owen, L., Browder, J., Letham, B., Stocek, G., Tymms, C., Shvartsman, M.: Adaptive nonparametric psychophysics. arXiv (2021). https://doi.org/10.48550/ARXIV.2104.09549